Rare Metal Materials and Engineering
Volume 51, Issue 10, October 2022
Available online at www.rmme.ac.cn

Science Press

Cite this article as: Li Ben, Cai Guangyu. Preparation Quality Characterization of Ni-based Single Crystal Alloy with Gas Film Pore Structure[J]. Rare Metal Materials and Engineering, 2022, 51(10): 3554-3562.

ARTICLE

Preparation Quality Characterization of Ni-based Single Crystal Alloy with Gas Film Pore Structure

Li Ben, Cai Guangyu

School of Intelligent Manufacturing, Nanyang Institute of Technology, Nanyang 473500, China

Abstract: The preparation quality of Ni-based single crystal alloy (NSCA) with gas film pore structure has become a key factor restricting the application and development of high-performance aero-engine equipment. However, due to the difficulty of quantitatively expressing the microstructure changes during the preparation process, it is difficult to quantitatively evaluate the preparation quality under different processes. In the present study, taking the advantages of ultrasonic guided wave that is sensitive to metal material micro-damage and has high detection efficiency and detection accuracy, excitation frequency (2.05 MHz) and benchmark characteristic parameters (7.58 e^{-4}/mm) of NSCA are determined, and then the influence mechanism of different preparation quality defects on the nonlinear parameters of guided wave is clarified by theoretical and experimental analysis, which will provide theoretical basis research for the subsequent efficient and controllable preparation of NSCA with gas film pore structure.

Key words: Ni-based single crystal alloy; gas film pore structure; laser-made hole; molecular dynamics

Owing to the excellent high-temperature mechanical properties and periodic microstructure and single crystal orientation (Fig.1)[1-3], Ni-based single crystal alloy (NSCA) is often used for high-performance aero-engine turbine blades[4,5]. In the process of preparing gas film pore structure on the surface of NSCA, it is easy to form some defects such as built-up edge, heat-affected zone and micro-cracks (Fig.2), which will greatly affect the service life of the material. At present, the evaluations of these defects are mostly macroscopic and most of them are qualitative evaluations. There is a lack of effective means to characterize the evolution of microstructure and it is difficult to express quantitatively. In mass production, particularly, it is hard to quantitatively evaluate the preparation quality of each component. As for NSCA components with air film pores, researches on the evaluation of preparation quality are mostly focused on the characterization of macro-defects (relying on ultrasonic body wave). The macro-cracks around the air film pore structure can be detected by ultrasonic body wave, based on which the macro-cracks can be characterized quantitatively. However, microcracks and macrocracks exist at the same time, and it is obvious that there is a certain degree of one-sidedness when only characterizing macro-cracks. There are plenty of macro-cracks on NSCA with gas film pore structure, which has a great impact on the service life. In the later service process, NSCA may fracture at any time under the influence of harsh service environments, and thus the characterization of macro-cracks is difficult to meet service requirements, and it is highly necessary to find efficient evaluation methods for the preparation quality of NSCA with gas film pore structure in the earlier stage.

Non-linear ultrasonic guided wave technology can over-

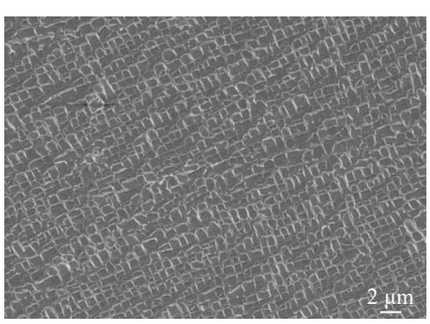

Fig.1 Microstructure of NSCA

Received date: October 07, 2021
Foundation item: China Postdoctoral Science Foundation (2021M691014); Project of Startup Foundation for Doctoral Research of Nanyang Institute of Technology (NGBJ-2020-02); Project for Interdisciplinary Scientific Research of Nanyang Institute of Technology (2021)
Corresponding author: Cai Guangyu, Ph. D, Professor, Nanyang Institute of Technology, Nanyang 473500, P. R. China, E-mail: caiguangyu71@163.com

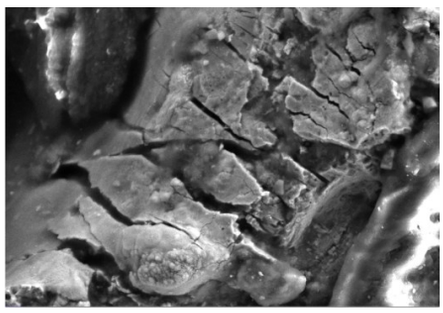

Fig.2 Micro-crack defect morphology around the gas film pore structure

come the shortcomings of traditional ultrasonic evaluation for micro-defects[6-13], which provides a new way to evaluate the microstructure evolution behavior of NSCA with air film pore structure[14,15]. In the preparation process of NSCA with gas film pore structure, nonlinear ultrasonic guided waves can be used to characterize the heat-affected zone, built-up edge, plenty of macro-cracks and micro-cracks, etc, which can fully meet the evaluation requirements for the preparation quality of air film pore structure. Ultrasonic guided wave nonlinear parameter can be incorporated into physical quantities that characterize the microstructure evolution behavior of NSCA with air film pore structure, by which the material microstructure evolution can be further expressed. Among the ultrasonic guided wave[16] (Lamb wave, SH wave, surface wave, Stonely wave, etc.) detection technology, Lamb wave has the advantages of being sensitive to the change of metal material microstructure, high detection efficiency and accuracy, especially suitable for the detection of blade-like plate materials. Based on this, it is necessary to analyze the influence mechanisms of amplitude characteristic parameters under mechanical and laser pitting processes, and to establish the corresponding amplitude characteristic parameter of NSCA with qualified preparation quality under experimental conditions.

1 Theoretical Analysis

There is a big difference between the mechanism of laser pitting and mechanical pitting. A certain volume of deposits will be formed on the surface of NSCA by laser pitting, the microstructure of which is quite different from that of base material, and the effect of them on the amplitude ratio characteristic parameter is similar to that of the precipitates. Meanwhile, there is almost no dislocation movement in the laser pitting process and few dislocations form around the pit, and the corresponding dislocation density is extremely small. Therefore, in the process of laser pitting, the dislocation density has little effect on the amplitude ratio characteristic parameter, and it is the surface precipitates that have a prominent effect on the amplitude ratio characteristic parameter. As for mechanical pitting, it is completely different from laser pitting. The process of mechanical pitting is mainly based on the movement of dislocations, which will form a large number of dislocations around the pit. Therefore, the dislocation density cannot be ignored, and in the process of mechanical pit making, the main influence on the formation of the amplitude ratio characteristic parameter is the dislocation. However, dislocations and precipitated phases exist almost at the same time. Therefore, in order to effectively characterize the amplitude ratio characteristic parameter of laser pitting and mechanical pitting, it is necessary to find a physical quantity that can simultaneously fuse dislocations and precipitated phase volume fractions.

Based on Ref. [17], the ratio of second harmonic displacement amplitude (A_{2f}) to the square of fundamental frequency displacement amplitude (A_{1f}^2) can be expressed by the following theoretical relationship:

$$\frac{A_{2f}}{A_{1f}^2} = \frac{ak^2(48\sigma R^3 E_1{}^3 \Omega L^4 \Lambda + 5\mu^3 b^2 E_2)}{80E_1\mu^3 b^2} \quad (1)$$

where a is the Lagrangian coordinate, k is the wave number, σ is the internal stress, R is the tangential decomposition factor, E_1 is the second-order elastic constant of NSCA, Ω is the conversion coefficient from the shear strain to the longitudinal strain, L is half of the dislocation chord length, Λ is the formed dislocation density, μ is the shear modulus of NSCA, b is Berman vector, and E_2 is the third-order elastic constant of NSCA. In Eq.(1), there is a lack of physical quantities that can characterize the volume fraction of deposits formed by laser pitting on the surface of NSCA. And the theoretical relationship between the volume fraction of deposits and the amplitude ratio characteristic parameters will be established.

Assuming that the internal stress of NSCA sample is σ, it has a theoretical relationship with the volume fraction of deposits[18], as follows:

$$\sigma = 2\varepsilon\mu f_p \quad (2)$$

where ε is the strain caused by stress concentration. Combining Eq.(1) and Eq.(2), a theoretical relationship can be established as follows:

$$\frac{A_{2f}}{A_{1f}^2} = \frac{ak^2(96\varepsilon f_p R^3 E_1{}^3 \Omega L^4 \Lambda + 5\mu^2 b^2 E_2)}{80E_1\mu^2 b^2} \quad (3)$$

The volume fraction of deposits formed on the surface of NSCA has been incorporated into the amplitude ratio characteristic parameter expression of Eq. (3). The establishment of this theoretical relationship can provide theoretical guidance for the change mechanism analysis of amplitude ratio characteristic parameters under the subsequent laser and mechanical pitting processes.

2 Experimental Method

2.1 Molecular dynamics simulation

It can be found from Eq. (3) that the amplitude ratio characteristic parameter is proportional to the dislocation density, and the larger the dislocation density, the larger the amplitude ratio characteristic parameter. For the change mechanism analysis of amplitude ratio characteristic parameter under the mechanical pitting process, because the variation of dislocation is the largest, the change trend of

dislocation density is the main factor affecting the amplitude ratio characteristic parameter. However, the dislocation density cannot be calculated accurately under the current experimental conditions, and the change trend of dislocation density also cannot be determined. Therefore, the change mechanism of amplitude ratio characteristic parameter under the mechanical pitting process cannot be effectively explained. The dislocation density and its change trend at the microscopic level can be accurately calculated using molecular dynamics method, based on which the basic molecular dynamics model built is shown in Fig.3.

2.2 Lamb wave propagation characteristic experiments

When evaluating the preparation quality of NSCA with gas film pore structure, it is necessary to verify the sensitivity of Lamb wave (second harmonic) to the micro-pit defect. If the second harmonic is not sensitive to the increase of micro-damages (laser-made micro-pits and mechanical micro-pits), it loses the significance to study the material damage. Therefore, the sensitivity of the second harmonic to micro-damage through experiments was first verified.

The experimental material was DD6 NSCA, and micro-pits with a diameter of 25 μm were prepared on the surface of each sample by laser-made pit technology. The number of laser pits in the 4 samples was 2, 4, 8, and 12, corresponding to sample 1#~4#, respectively. Due to the small number of laser pits, the distance between the transmitter and the receiver was set to 2 cm. The Lamb wave experimental system (Model RAM-5000-SNAP) was used for testing, the incident and receiving angles were both 19.5°, and the optimal excitation frequency was 2.05 MHz.

As for mechanical micro-pits, the diamond-shaped pits with a side length of 25 μm were prepared on the surface of each sample by mechanical indentation technology. In order to fully study the sensitivity of Lamb wave to the micro-defects, a total of 4 samples were made. The shape of pits on the surface of each sample was same, but the number of pits was different. The degree of sensitivity of Lamb wave to micro-defects was judged through the increasing number of pits. Among the 4 samples, the number of mechanical pits was 2 (5# sample), 4 (6# sample), 8 (7# sample), 12 (8# sample). The experimental conditions were the same as defined above.

Since Lamb wave is sensitive to micro-defects, parasitic signals or other interference signals may be mixed during the experiment, which will have a great impact on the generation efficiency of the second harmonic. Therefore, in order to reduce the experimental error as much as possible, it is necessary to eliminate the interference of parasitic signals and other interference signals before experiment. At present, the amplitude ratio characteristic parameter (the ratio of the second harmonic displacement amplitude to the square of the fundamental frequency displacement amplitude) is generally applied for effectively judging whether other signals are mixed in. This is because in the absence of interference signals, the amplitude ratio characteristic parameter is a certain value. As for NSCA with gas film pore structure, the preparation quality evaluation will be expressed by the amplitude ratio characteristic parameter. In order to effectively distinguish the air film pore structure of different preparation quality, the air film pore structures were prepared with different emission powers. After many tests, it was found that when the emission power reaches 16 W, a complete air film pore structure could be formed, and the corresponding amplitude ratio characteristic parameter could be used as a reference characteristic parameter. When the emission power was below 16 W, there were some shallow deformed pits. For the purpose of fully verifying whether the air film pore structure of different preparation quality can be effectively distinguished based on the amplitude ratio characteristic parameter, the same number (100) of air film pore structures were prepared on the surface of sample 9#~12# (corresponding powers were 7, 10, 13, 16 W respectively) with different emission powers. Then the samples were tested by Model RAM-5000-SNAP system, and the corresponding amplitude ratio characteristic parameters were obtained after post-processing. By comparing and analyzing the difference between the amplitude ratio characteristic parameters, the feasibility of preparation quality characterizing of NSCA with air film pore structure based on the amplitude ratio characteristic parameter will be fully judged.

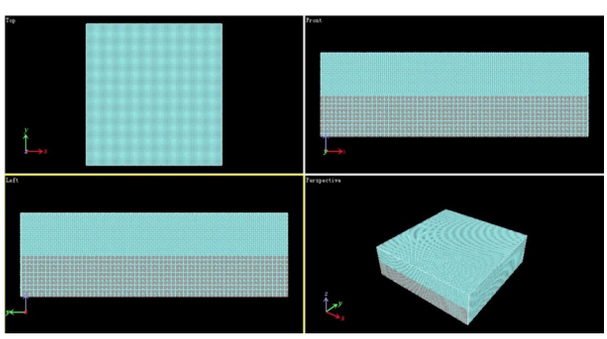

Fig.3 Basic molecular dynamics model of NSCA

3 Results and Discussion

The morphology of laser pits on the surface of sample 1# is shown in Fig. 4a. Two micro-pits with an aperture of 25 μm can be clearly seen on the sample surface. The time-domain and frequency-domain signals are shown in Fig. 5a. Obviously, the elliptical waveforms can be observed, the second harmonic displacement amplitude is 0.034 mm, and the amplitude ratio characteristic parameter is 0.94 e^{-4}/mm. Ref. [19] studied the influence of propagation distance on the propagation characteristics of Lamb wave in NSCA. When the propagation distance between the transmitting end and the receiving end is 2 cm (the incident and receiving angles are both 19.5°, the excitation frequency is 2.05 MHz), the second harmonic displacement amplitude is 0.024 mm, and the amplitude ratio characteristic parameter is 0.66 e^{-4}/mm. In comparison with the experimental results in Ref. [19], when two laser pits are added on the surface of NSCA, the second harmonic displacement amplitude is increased by 0.010 mm, and the amplitude ratio characteristic parameter is increased

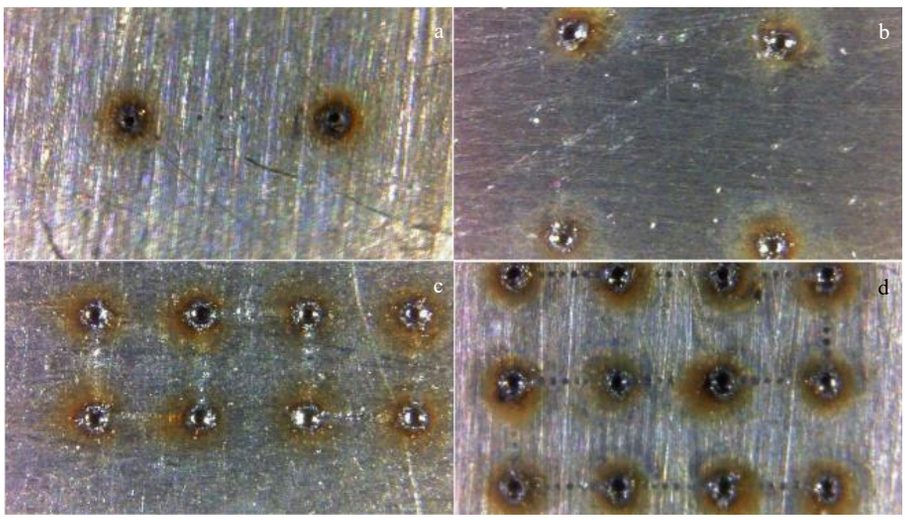

Fig.4 Morphologies of laser pits on the surface of different samples: (a) 1#, (b) 2#, (c) 3#, and (d) 4#

by 0.28 e^{-4}/mm, which indicates that Lamb wave is sensitive to micro-defects such as laser pits.

The morphology of laser pits on the surface of 2# sample is shown in Fig. 4b. There are four laser pits on the sample surface. The time-domain and frequency-domain signals are shown in Fig. 5b. Obviously, the elliptical waveforms can be also observed, the corresponding second harmonic displacement amplitude is 0.046 mm, and the amplitude ratio characteristic parameter is 1.27 e^{-4}/mm. In comparison with the experimental results in Fig. 5a, it is found that the number of laser pits increases from two to four, the second harmonic displacement amplitude is increased by 0.012 mm, and the amplitude ratio characteristic parameter is increased by 0.33 e^{-4}/mm.

The morphology of laser pits on the surface of 3# sample is shown in Fig. 4c. There are eight array micro-pits on the sample surface. The time-domain and frequency-domain signals are shown in Fig. 5c, the second harmonic displacement amplitude is 0.065 mm, and the amplitude ratio characteristic parameter is 1.80 e^{-4}/mm. In comparison with the experimental results in Fig. 5b, it is found that when four laser pits are added, the corresponding second harmonic displacement amplitude is increased by 0.021 mm, and the amplitude ratio characteristic parameter is increased by 0.58 e^{-4}/mm.

The morphology of laser pits on the surface of sample 4# is shown in Fig. 4d. Twelve array micro-pits can be clearly observed on the sample surface. The time-domain and

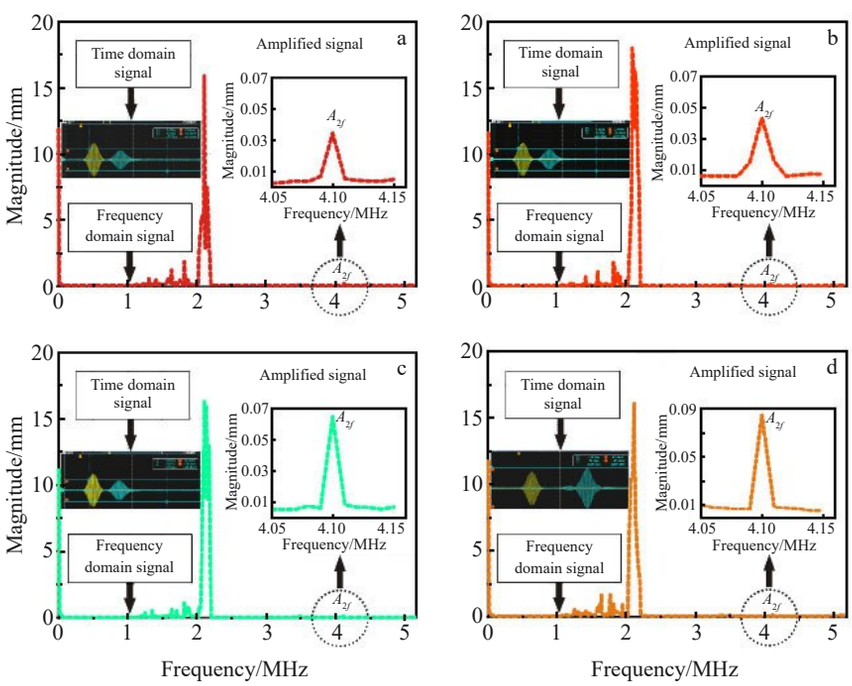

Fig.5 Time-domain and frequency-domain signals of different samples: (a) 1#, (b) 2#, (c) 3#, and (d) 4#

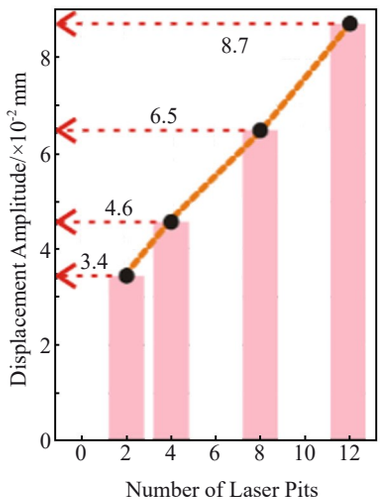

Fig.6 Relationship curve between the second harmonic displacement amplitude and the number of laser pits

frequency-domain signals are shown in Fig. 5d, the second harmonic displacement amplitude is 0.087 mm, and the amplitude ratio characteristic parameter is 2.41 e^{-4}/mm. In comparison with the experiment results in Fig. 5c, it is found that when the number of laser pits increases from 8 to 12, the second harmonic displacement amplitude is increased by 0.022 mm, and the amplitude ratio characteristic parameter is increased by 0.61 e^{-4}/mm. The above four sets of ultrasonic experimental results show that as the number of laser pits increases, the corresponding second harmonic displacement amplitude and the amplitude ratio characteristic parameter increase significantly (Fig.6), which indicates that Lamb wave is sensitive to micro-defects. The experimental results and research results of Ref.[19] can be mutually corroborated.

In summary, a certain volume of deposits can be formed on the surface of NSCA after laser pitting, and the volume of deposits increases with the increase of the number of pits. According to the acoustic experiment results and the theoretical formula of Eq. (3), it can be concluded that the constant increase of amplitude ratio characteristic parameter is mainly caused by the increase of the volume fraction of deposits.

The micro-morphology of mechanical indentations on the surface of sample 5# is shown in Fig. 7a. There are two diamond-shaped mechanical indentations on the sample surface. Fig. 8a shows the time-domain and frequency-domain signals. The elliptical waveforms can be observed, and the second harmonic signal is clear. At this time, the second harmonic displacement amplitude is 0.028 mm. In comparison with the experimental results in Ref. [19], the corresponding second harmonic displacement amplitude of NSCA from defect-free state to defective state (2 diamond-shaped pits with a side length of 25 μm) is increased by 0.004 mm, which indicates that Lamb wave is sensitive to such defects. After further calculation and comparison, it is found that when the second harmonic displacement amplitude increases, the corresponding amplitude ratio characteristic parameter increases from 0.66 e^{-4}/mm to 0.77 e^{-4}/mm.

The micro-morphology of mechanical indentations on the surface of sample 6# is shown in Fig. 7b. Four diamond-shaped mechanical indentations can be clearly seen on the sample surface. In comparison with Fig. 7a, the number of diamond-shaped mechanical indentations is increased by 2. The time-domain and frequency-domain signals are shown in Fig. 8b. Obvious elliptical waveforms can be also observed, the second harmonic displacement amplitude is 0.034 mm, and the amplitude ratio characteristic parameter is 0.94 e^{-4}/mm. In comparison with the experimental results in Fig. 8a, it is found that after two diamond-shaped mechanical

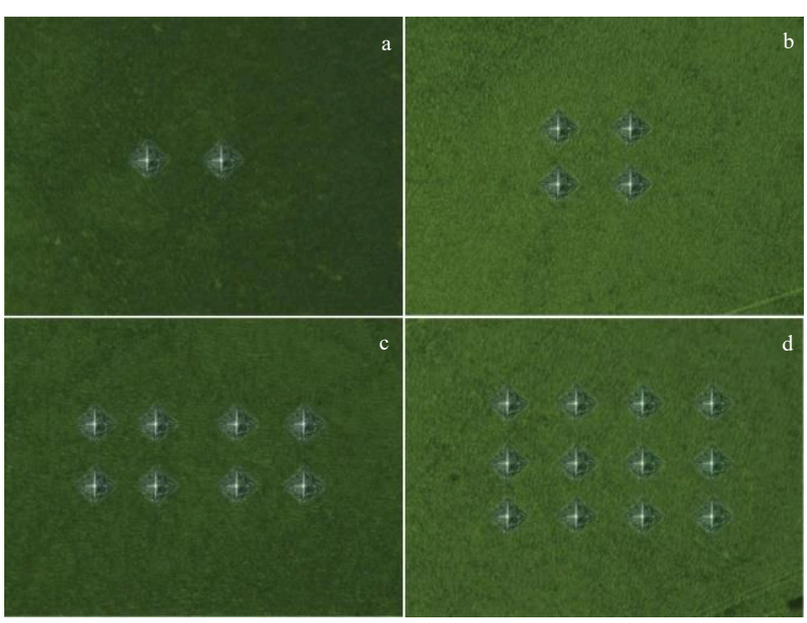

Fig.7 Morphologies of mechanical indentations on the surface of different samples: (a) 5#, (b) 6#, (c) 7#, and (d) 8#

indentations are added to the sample surface, the second harmonic displacement amplitude is increased by 0.006 mm, and the amplitude ratio characteristic parameter is increased by 0.17 e^{-4}/mm.

The micro-morphology of mechanical indentation on the surface of the 7# sample is shown in Fig. 7c. There are eight diamond-shaped mechanical indentations on the sample surface. In comparison with Fig. 7b, the number of diamond-shaped mechanical indentations is increased by 4. The time-domain and frequency-domain signals are shown in Fig. 8c. The second harmonic displacement amplitude is 0.045 mm, and the amplitude ratio characteristic parameter is 1.24 e^{-4}/mm. In comparison with the experimental results in Fig. 8b, it is found that after adding 4 diamond-shaped mechanical indentations on the sample surface, the corresponding second harmonic displacement amplitude is increased by 0.011 mm, and the amplitude ratio characteristic parameter is increased by 0.30 e^{-4}/mm.

The micro-morphology of mechanical indentation on the surface of the sample 8# is shown in Fig. 7d. Twelve diamond-shaped mechanical indentations can be clearly seen on the sample surface. Fig. 8d shows the time-domain and frequency-domain signals. The second harmonic displacement amplitude is 0.063 mm, and the amplitude ratio characteristic parameter is 1.74 e^{-4}/mm. In comparison with the experimental results in Fig. 8c, it is found that after adding 4 diamond-shaped mechanical indentations on the sample surface, the corresponding second harmonic displacement amplitude is increased by 0.016 mm, and the amplitude ratio characteristic parameter is increased by 0.44 e^{-4}/mm, which indicates that Lamb waves are sensitive to micro-defects. In summary, the second harmonic displacement amplitude increases with the increase in the number of mechanical indentations, as shown in Fig. 9. The above experimental results indicate that Lamb wave is highly sensitive to micro-defects formed by laser-made micro-pits and mechanical micro-pits, which can provide a good foundation for the subsequent use of amplitude ratio characteristic parameter to characterize the preparation quality of NSCA with air film pore structure.

The change mechanism of the amplitude ratio characteristic parameter under mechanical pitting is analyzed as follows. It can be found from Eq. (3) that the amplitude ratio characteristic parameter is proportional to the dislocation density. And it has been analyzed above that the dislocation movement under the mechanical pitting is the main factor affecting the amplitude ratio characteristic parameter. Therefore, it is necessary to analyze the change characteristics of dislocation density under the mechanical pitting. Fig. 10 displays the state diagrams of the three-dimensional molecular dynamics model of NSCA (modeling method is consistent with the research results in Ref. [20-22]) under mechanical pitting (atom distribution states under different pressure depths). Fig. 11a~11f shows the dislocation distributions corresponding to the states in Fig. 10a~10, respectively. Fig. 10a presents the atom distribution state when the mechanical press-in has not yet started. It can be found from Fig. 11a that no new dislocations are added. Fig. 10b displays the atom distribution state when the simulated mechanical indentation depth reaches 0.7 nm (the indentation radius of the simulated diamond indenter is set to 0.6 nm). It can be found from Fig. 11b that the dislocations have been added to the 3D model. After statistical analysis in the Ovito system (the analysis method is similar to the method used in Ref. [23,24]), a total of 57 dislocations with various types are formed in the 3D model. The total chord length of the dislocation is calculated, which is 213 nm, and the corresponding

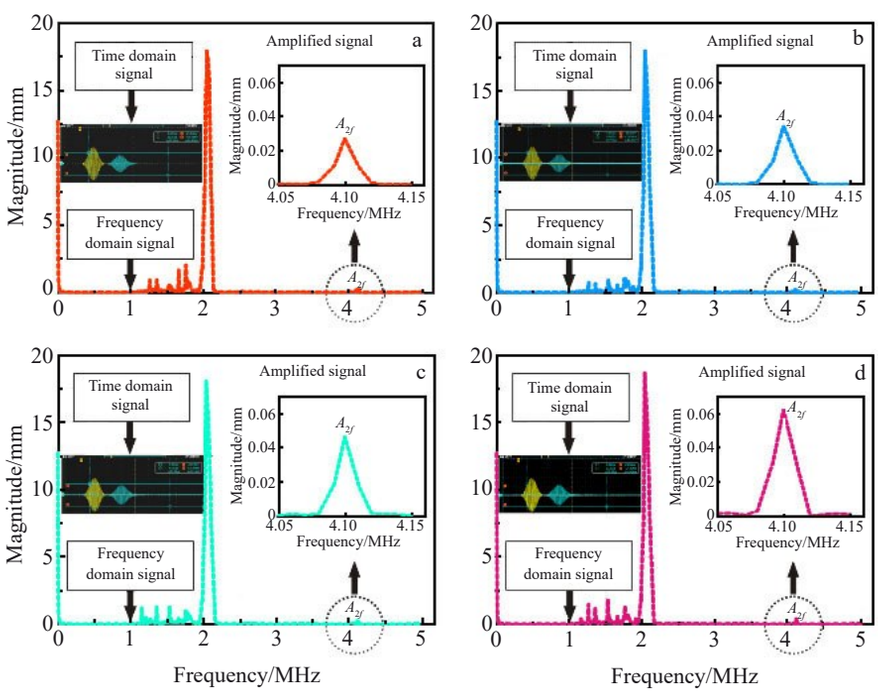

Fig.8 Time-domain and frequency-domain signals of different samples: (a) 5#, (b) 6#, (c) 7#, and (d) 8#

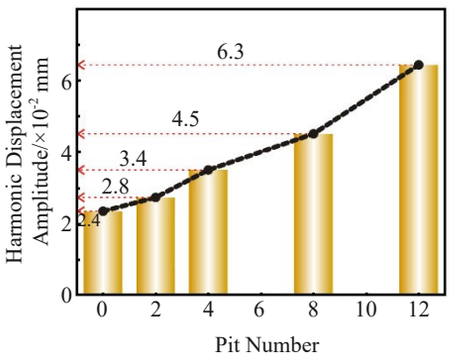

Fig.9 Variation curves of the amplitude of second harmonic displacement with the number of mechanical indentation

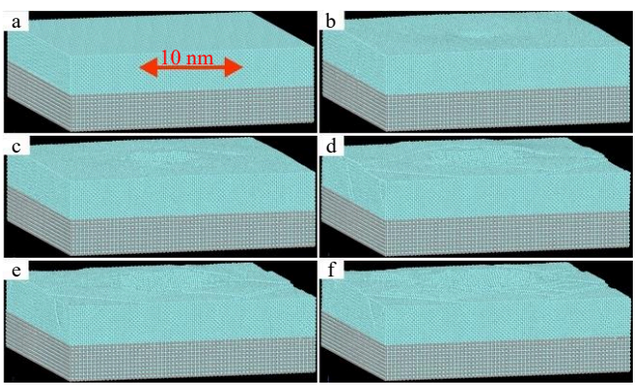

Fig.10 Distribution of atoms under different press depth conditions: (a) 0 nm, (b) 0.7 nm, (c) 1.4 nm, (d) 2.1 nm, (e) 2.8 nm, and (f) 3.5 nm

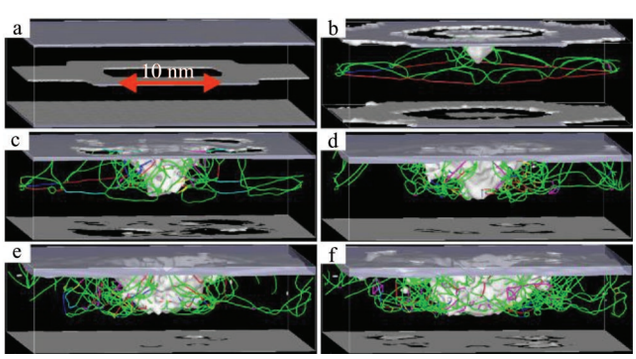

Fig.11 Dislocation distribution state corresponding to Fig. 10 under different press depth conditions: (a) 0 nm, (b) 0.7 nm, (c) 1.4 nm, (d) 2.1 nm, (e) 2.8 nm, and (f) 3.5 nm

dislocation density is 5.56 e^{16}/m^{-2}. Fig. 10c shows the atom distribution when the simulated mechanical indentation depth reaches 1.4 nm. According to Fig. 11c, the Ovito system analysis indicates that a total of 193 dislocations are formed. The total length of the dislocation is 359.9 nm, and the corresponding dislocation density is 9.39 e^{16}/m^{-2}, which increases significantly with the pressure depth. Fig. 10d displays the atomic distribution state when the simulated mechanical indentation depth reaches 2.1 nm. According to Fig. 11d, a total of 321 dislocations are formed through statistical analysis. The total length of the dislocation is 491.5 nm, and the dislocation density further increases to 12.83 e^{16}/m^{-2}. Fig. 10e displays the atom distribution state when the simulated mechanical indentation depth reaches 2.8 nm. It can be found from Fig. 11e that the dislocation density is relatively high. After statistical analysis, the total length of the dislocation is 503.4 nm, and the dislocation density increases to 13.13 e^{16}/m^{-2}. Fig. 10f shows the atom distribution state when the simulated mechanical indentation depth reaches 3.5 nm. According to Fig. 11f, the total length of dislocations is 770.1 nm, and the corresponding dislocation density further increases to 20.10 e^{16}/m^{-2}.

According to the analysis of the above simulation calculation results, the dislocation density of NSCA under mechanical pitting is an increasing process, which is consistent with the research results in Ref. [19]. It can be found from Eq. (3) that the amplitude ratio characteristic parameter is proportional to the dislocation density. Therefore, the corresponding amplitude characteristic parameter increases with the increase of dislocation density, which can well explain the change mechanism of the amplitude ratio characteristic parameter in the above mechanical pitting experiment.

The gas film pore structures prepared on the surface of NSCA samples (a total of four kinds of structures correspond to sample 9#~12#) are shown in Fig. 12. In order to effectively distinguish the unqualified and qualified air film pore structures and use the amplitude ratio characteristic parameter to evaluate the difference, different emission powers are used to prepare the air film pore structures (the preparation method of air film pore structure is similar to the preparation method in Ref. [25, 26]). The corresponding laser emission powers of sample 9#~12# are 7, 10, 13 and 16 W, respectively. The micro-morphologies of the air film pore structures of sample 9#~12# are shown in Fig. 13. It can be found that when the laser emission power is lower than 16 W, a complete air film pore structure cannot be formed, and the preparation quality can be regarded as unqualified. If there is a big difference in the amplitude ratio characteristic parameters corresponding to the qualified and unqualified gas film pore structures, it can be indicated that it is feasible to use the amplitude ratio characteristic parameter to characterize the preparation quality of NSCA with gas film pore structure.

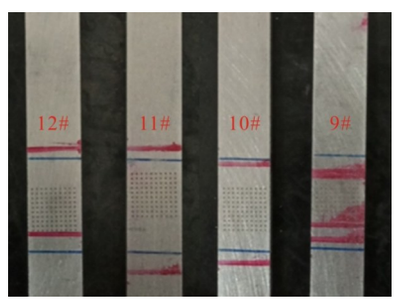

Fig.12 Air film pore structure samples prepared with different emission powers

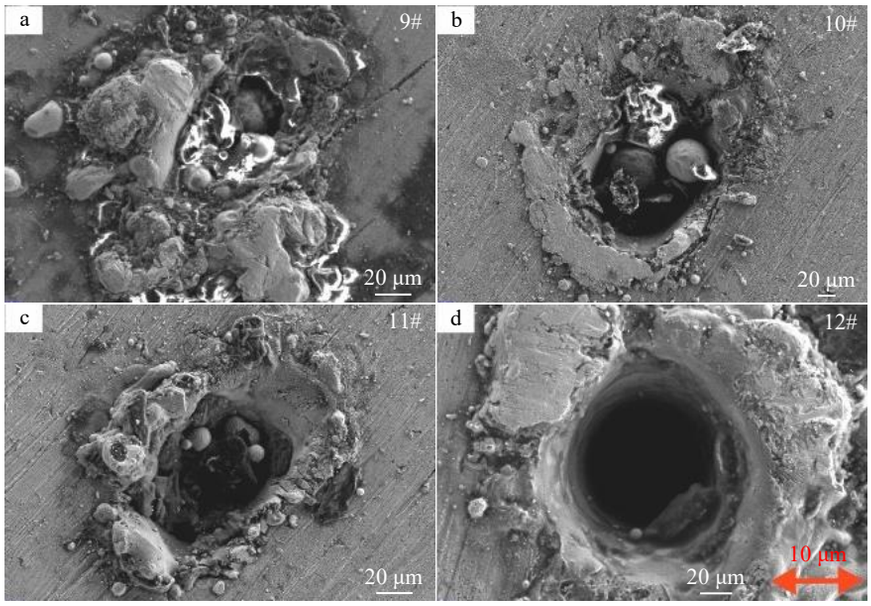

Fig.13 Micro-morphologies of air film pore structure on each group of samples: (a) 9#, (b) 10#, (c) 11#, and (d) 12#

The change trend of amplitude ratio characteristic parameters corresponding to sample 9#~12# is shown in Fig.14. The amplitude ratio characteristic parameter of sample 9# (laser emission power is 7 W) is 3.33 e^{-4}/mm. When the laser emission power increases from 7 W to 10 W, the amplitude ratio characteristic parameter of sample 10# increases to 4.49 e^{-4}/mm. It can be found that the larger the emission power, the larger the volume of deposits, which has a greater impact on the amplitude ratio characteristic parameter. When the laser emission power increases from 10 W to 13 W, the amplitude ratio characteristic parameter of sample 11# increases to 5.49 e^{-4}/mm. And when the transmitting power continues to increase to 16 W, the amplitude ratio characteristic parameter of sample 12# is 7.58 e^{-4}/mm. In summary and according to the research results in Ref. [19], it can be concluded that the second harmonic displacement amplitude is closely related to the volume of deposits or precipitates formed during the process of laser-made hole. Under the cumulative growth characteristics, the nonlinear factor is enhanced as the volume of deposits becomes larger, and the average energy flow used to supply the second harmonic generation increases, that is the sum of the surface energy flow and the body energy flow increases. Therefore, the second harmonic displacement amplitude increases, and the corresponding amplitude ratio characteristic parameter increases.

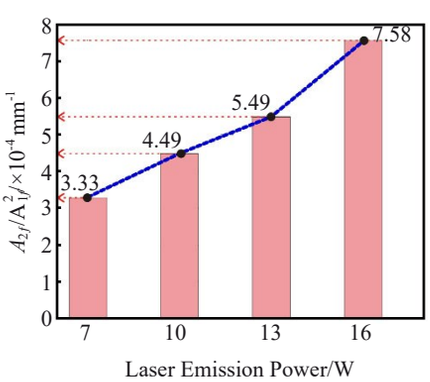

Fig.14 Change trend of amplitude characteristic parameters corresponding to each group of samples

Based on the above analysis, it can be found that there is a big difference in the amplitude ratio characteristic parameters corresponding to NSCA with gas film pore structures of qualified and unqualified preparation quality, according to which the preparation quality of the material can be quickly determined. When the preparation quality is qualified, the corresponding amplitude ratio characteristic parameter is 7.58 e^{-4}/mm (the benchmark amplitude ratio characteristic parameter), which can be used as a criterion for judging the preparation quality of NSCA with gas film pore structure (simulation criterion under the experimental conditions). Accordingly, it is feasible to use the amplitude ratio characteristic parameter to characterize the preparation quality of NSCA with gas film pore structure.

4 Conclusions

1) Theoretical analysis shows that the amplitude ratio characteristic parameter under the mechanical pitting process is mainly affected by the dislocation density and proportional to dislocation density.

2) In the laser pitting process, the amplitude ratio characteristic parameter is mainly affected by the volume fraction of deposits and proportional to it.

3) The greater the laser emission power, the larger the volume of deposits formed around the gas film pore structure, and the bigger the corresponding amplitude ratio characteristic parameter.

4) There is a big difference in the amplitude ratio

characteristic parameters corresponding to NSCA with gas film pore structures of qualified and unqualified preparation quality, which can be used (the benchmark amplitude characteristic parameter is 7.58 e^{-4}/mm) as a criterion to determine the preparation quality of NSCA with gas film pore structure (simulation criteria under experimental conditions).

References

1 Zhao G Q, Tian S G, Shu D L *et al. Materials Research Express* [J], 2020(7): 66 507
2 Wang X H, Zhang J L, Chen D P *et al. Rare Metal Materials and Engineering*[J], 2020, 49(10): 348
3 Lemos G, Farina A B, Nunes R M *et al. Journal of Materials Research and Technology*[J], 2019, 8(1): 2528
4 Long H, Liu Y, Mao S *et al. Intermetallics*[J], 2018, 94: 55
5 Cantrell J H. *P Roy Soc A-Math Phys*[J], 2004, 460: 757
6 Lou Z J, Liu H, Yang G J *et al. J Alloy Compd*[J], 2021, 861: 158 589
7 Deng M X, Xiang Y, Liu L B. *J Appl Phys*[J], 2011, 109: 1829
8 Deng M X, Xiang Y X, Liu L B. *Chin Phys B*[J], 2010, 28: 456
9 Xiang Y X, Deng M X, Xuan F Z *et al. Ndt & E Int*[J], 2011, 44: 768
10 Buck O, Morris W L, Richardson J M. *Appl Phys Lett*[J], 1978, 33(5): 371
11 Deng M. *Appl Phys Lett*[J], 2006, 88: 13
12 Deng M. *Ndt & E Int*[J], 2005, 38: 85
13 Deng M, Wang P, Lv X. *Appl Phys Lett*[J], 2005, 86: 287
14 Zhu W J, Xiang Y X, Liu C J *et al. Ultrasonics*[J], 2018, 90: 18
15 Shih C C, Qian X J, Ma T *et al. IEEE T Med Imaging*[J], 2018, 37: 1887
16 Huang C Y, Sun J H, Wu T T. *Appl Phys Lett*[J], 2010, 97: 162
17 Zhang H, Zhang J, Fan G *et al. Metals-Open Access Metallurgy Journal*[J], 2019, 9(6): 666
18 Chen H, Liu Z, Gong Y *et al. IEEE Transactions on Ultrasonics Ferroelectrics and Frequency Control*[J], 2021, 99: 1
19 Li B, Liu R, Zhu W *et al. Applied Surface Science*[J], 2019, 483: 840
20 Li B, Zhang S M, Essa F A *et al. Rare Metal Materials and Engineering*[J], 2018, 47(5): 1370
21 Li B, Dong C, Yu J G *et al. RSC Advances*[J], 2018, 8(39): 22 127
22 Yu J G, Zhang Q X, Liu R *et al*. *RSC Advances*[J], 2014, 4(62): 32 749
23 Li J. *Modelling and Simulation in Materials Science and Engineering*[J], 2003, 11: 173
24 Stukowski A. *Modelling and Simulation in Materials Science and Engineering*[J], 2010, 18: 15 012
25 Wen Z X, Zhang D X, Li S W *et al. J Alloy Compd*[J], 2017, 692: 301
26 Wen Z X, Pei H Q, Wang B Z *et al*. *Materials at High Temperatures*[J], 2016, 33: 68

镍基单晶合金气膜孔结构的制备质量评价

李　本，蔡广宇

(南阳理工学院 智能制造学院，河南 南阳 473500)

摘　要：镍基单晶合金（NSCA）气膜孔结构制备质量已成为制约高性能航空发动机装备应用和发展的关键因素，然而，由于制备过程中形成的微结构变化难以定量表达，很难对不同工艺下的制备质量进行定量评价。利用兰姆波对金属材料微损伤敏感的优势，结合分子动力学模拟分析了不同工艺下制备质量的影响机理，确立了NSCA合理的激发角度 （19.5°）、激发频率（2.05 MHz）及基准特征参数（7.58 e^{-4}/mm）。并通过理论和实验揭示了制备缺陷与二次谐波间的构效关系，为后续工程化应用提供理论依据。

关键词：镍基单晶合金；气膜孔结构；激光打孔；分子动力学

作者简介：李　本，男，1986年生，博士，南阳理工学院智能制造学院，河南 南阳 473500，E-mail：li_dd21@163.com